Sexual dimorphism in hepatic lipids is associated with the evolution of metabolic status in mice

Article *in* NMR in Biomedicine · June 2017

DOI: 10.1002/nbm.3761

5 authors, including:

Hongxia Lei
École Polytechnique Fédérale de Lausanne
79 PUBLICATIONS **1,087** CITATIONS

Research article

NMR IN BIOMEDICINE

Received: 25 November 2014, Revised: 19 May 2015, Accepted: 20 May 2015, Published online in Wiley Online Library: 28 June 2015

(wileyonlinelibrary.com) DOI: 10.1002/nbm.3345

Characterization of hepatic fatty acids in mice with reduced liver fat by ultra-short echo time ^{1}H-MRS at 14.1 T *in vivo*

Ana Francisca Soares[a]*, Hongxia Lei[b,c] and Rolf Gruetter[a,c,d]

Alterations in the hepatic lipid content (HLC) and fatty acid composition are associated with disruptions in whole body metabolism, both in humans and in rodent models, and can be non-invasively assessed by ^{1}H-MRS *in vivo*. We used ^{1}H-MRS to characterize the hepatic fatty-acyl chains of healthy mice and to follow changes caused by streptozotocin (STZ) injection. Using STEAM at 14.1 T with an ultra-short T_E of 2.8 ms, confounding effects from T_2 relaxation and *J*-coupling were avoided, allowing for accurate estimations of the contribution of unsaturated (UFA), saturated (SFA), mono-unsaturated (MUFA) and poly-unsaturated (PUFA) fatty-acyl chains, number of double bonds, PU bonds and mean chain length. Compared with *in vivo* ^{1}H-MRS, high resolution NMR performed *in vitro* in hepatic lipid extracts reported longer fatty-acyl chains (18 versus 15 carbons) with a lower contribution from UFA (61 ± 1% versus 80 ± 5%) but a higher number of PU bonds per UFA (1.39 ± 0.03 versus 0.58 ± 0.08), driven by the presence of membrane species in the extracts. STZ injection caused a decrease of HLC (from 1.7 ± 0.3% to 0.7 ± 0.1%), an increase in the contribution of SFA (from 21 ± 2% to 45 ± 6%) and a reduction of the mean length (from 15 to 13 carbons) of cytosolic fatty-acyl chains. In addition, SFAs were also likely to have increased in membrane lipids of STZ-induced diabetic mice, along with a decrease of the mean chain length. These studies show the applicability of ^{1}H-MRS *in vivo* to monitor changes in the composition of the hepatic fatty-acyl chains in mice even when they exhibit reduced HLC, pointing to the value of this methodology to evaluate lipid-lowering interventions in the scope of metabolic disorders.

Keywords: mouse liver; fatty acids; streptozotocin (STZ); magnetic resonance spectroscopy (MRS); poly-unsaturated fatty acids (PUFA)

INTRODUCTION

The liver plays a pivotal role in whole body energy balance, being actively involved in lipid handling. Accumulation of lipids in the liver (steatosis) perturbs normal hepatic metabolism (1) and is associated with insulin resistance, obesity and metabolic syndrome (2–5). On the other hand, depletion of hepatic lipids may also occur in cases of metabolic imbalances, such as in animal models of type 1 diabetes (6,7). Changes in the hepatic lipid content (HLC) are often accompanied by alterations in the relative contributions of saturated, mono-unsaturated and poly-unsaturated fatty acids (SFA, MUFA and PUFA, respectively) to the acyl chains of hepatic lipids. In humans, steatosis is associated with a depletion of hepatic PUFA (8), and a diet enriched in PUFA has been shown to protect against hepatic fat accumulation in both humans (9) and rodents (10). Alterations in the composition of hepatic and circulating lipids have also been observed in rodent models of streptozotocin (STZ)-induced type 1 diabetes (11,12).

Therefore, addressing the hepatic lipids in mice is of interest for many models of metabolic disorders also present in humans, as it may bring important insight to mechanisms of disease or outcome of pharmacological and/or dietary interventions. In this context, the longitudinal characterization of hepatic fatty acids may be non-invasively performed by ^{1}H-MRS *in vivo* since the different types of proton in these chains give rise to resonances at specific chemical shifts in the ^{1}H-MR spectrum (13–15). Point-resolved spectroscopy (PRESS) and stimulated echo-acquisition mode (STEAM) are single-scan localization ^{1}H-MRS sequences widely used to measure hepatic lipids *in vivo* (16), and both have been validated against biochemical and histological quantifications of lipids in hepatic tissue in humans and animal models (17–22). PRESS has been the preferred technique to study mice

* *Correspondence to: A. F. Soares, Laboratory for Functional and Metabolic Imaging (LIFMET), École Polytechinque Fédérale de Lausanne (EPFL), Lausanne, Switzerland. E-mail: francisca.soares@epfl.ch*

a *A. F. Soares, R. Gruetter*
Laboratory for Functional and Metabolic Imaging (LIFMET), École Polytechinque Fédérale de Lausanne (EPFL), Lausanne, Switzerland

b *H. Lei*
Center for Biomedical Imaging (CIBM), Lausanne, Switzerland

c *H. Lei, R. Gruetter*
Department of Radiology, University of Geneva (UNIGE), Geneva, Switzerland

d *R. Gruetter*
Department of Radiology, Faculty of Biology and Medicine, University of Lausanne, Lausanne, Switzerland

Abbreviations used: *HLC, hepatic lipid content; HR-NMR, high resolution liquid state NMR; MCL, mean chain length; MUFA, mono-unsaturated fatty-acyl chains or fatty acids; ndb, number of double bonds; PO, peanut oil; PRESS, point-resolved spectroscopy; PtdCho, phosphatidylcholine; PU/FA, poly-unsaturated bonds per fatty-acyl chain; PU/UFA, poly-unsaturated bonds per unsaturated fatty acyl chain; PUFA, poly-unsaturated fatty-acyl chains or fatty acids; SFA, saturated fatty-acyl chains or fatty acids; SNR, signal-to-noise ratio; SO, sunflower oil; STZ, streptozotocin; STEAM, stimulated echo-acquisition mode; UFA, unsaturated fatty-acyl chains or fatty acids; VOI, volume of interest.*

(18,23–27) as, relative to STEAM, it has a potentially twofold improved sensitivity, hence allowing for higher signal-to-noise ratio (SNR). Even so, only a few studies have characterized hepatic fatty-acyl chains in hepatic lipids in non-steatotic mice with PRESS by taking advantage of high magnetic fields (25,27). Indeed, the reduced sample size and the nature of PRESS, a double spin echo sequence with a relatively long T_E (in the range of tens of milliseconds), compromise the detection of less abundant fatty-acyl protons in the mouse liver. Unlike PRESS, STEAM can reach a T_E as short as 1 ms (28), which, in combination with lower power requirements, makes STEAM most advantageous for determining the hepatic fatty acid composition from a deeper region.

The aim of this study was to quantify the HLC and characterize the fatty-acyl chains of hepatic lipids (including the relative contributions from SFA, PUFA and MUFA) in healthy mice using an ultra-short T_E STEAM at 14.1 T. These measurements were compared with those performed in liver tissue extracts by high resolution liquid state NMR (HR-NMR). Furthermore, we tested the power of the method in a model displaying reduced HLC, the STZ-induced diabetic mouse.

MATERIALS AND METHODS

Phantom studies

A soybean oil-in-water emulsion (Intralipid® 20%) was used to prepare standards of different lipid content by dilution in distilled water: 0.2%, 0.5%, 1%, 2.5%, 5%, 7.5%, 10% and 20%. Phantoms from sunflower oil (SO), peanut oil (PO) and respective mixtures (SO:PO 2:1, 1:1 and 1:2 v/v) were studied to assess the performance of the method for different fatty acid compositions. MR measurements were made with the same imaging and spectroscopy sequences and parameters as those used for the mouse experiments *in vivo*, as described below.

Animal studies

All experiments were approved by the local ethics committee (Service de la consommation et des affaires vétérinaires, Épalinges, Switzerland). C57BL/6J mice (Charles Rivers Laboratories, L'Arbresle, France) were housed in a 12 h light/12 h dark cycle with free access to water and a standard chow diet (Kliba-Nafag, Kaiseraugst, Switzerland) and allowed at least 1 week of acclimatization. Twelve mice (4–10 months of age) weighing 23.9–45.0 g were used in the study to validate HLC quantification by ^{1}H-MRS *in vivo*. Five mice 4 months of age (25.9 ± 0.7 g) were used to compare the hepatic fatty acid composition estimated from spectra acquired by ^{1}H-MRS *in vivo* with that estimated from spectra acquired from the respective liver extracts by HR-NMR *in vitro*. In another cohort, five mice (5 months, 32.4 ± 0.9 g) received a single 180 mg/kg intraperitoneal injection of STZ (Sigma-Aldrich, Basel, Zürich, Switzerland) dissolved in citrate buffer (10 mM, pH 4.5). Glycemia was measured from tail tip blood with a glucose meter (Breeze, Bayer, Zürich, Switzerland) and animals were considered diabetic with values above 15.0 mM. ^{1}H-MRS assessments were made before STZ injection and 7 and 14 days afterwards, and HR-NMR was performed in liver extracts for the last time point.

For *in vivo* MR studies, induction of anesthesia was done with 4% isoflurane in an air:oxygen mixture (70:30) for 2 min and maintained with 1–2% isoflurane throughout the MR experiment. Mice were transferred to a home-built holder equipped with circulating warm water and their body temperature maintained between 36 and 37 °C, as continuously assessed by a rectal probe. The respiratory rate was maintained between 60 and 90 bpm by regulating the isoflurane level and was continuously monitored by means of an air pillow through an MR-compatible system (SA Instruments, Stony Brook, NY, USA) that also delivered necessary triggering signals to the console for respiratory gating. After the last MR session, mice were immediately euthanized by decapitation; the livers were collected and immediately freeze clamped in liquid nitrogen and stored at −80 °C until further processing.

MR methods

Measurements were made in a horizontal bore 14.1 T–26 cm magnet interfaced to a Direct Drive console (VnmrJ, Agilent Technologies, Palo Alto, CA, USA). Mice were scanned in the supine position with a ^{1}H quadrature surface coil (two 13 mm inner diameter physically decoupled loops) placed above their abdomens. Automatic shimming to reduce magnetic field inhomogeneities was performed with FAST(EST)MAP (29). Multi-slice gradient echo images were acquired in the sagittal, axial and coronal orientations with a 85° flip angle, a field of view of 25 mm × 25 mm, a 128 × 128 data matrix, minimum T_R and minimum T_E. From these images a (2 × 2 × 2) mm^3 volume of interest (VOI) was selected and localized spectroscopy performed using STEAM, as previously described by Tkáč *et al*. (28), employing an asymmetric 500 μs 90° RF pulse that provided a 13.5 kHz bandwidth. At 600 MHz and with gradient strengths of approximately 100 mT/m, chemical shift displacement was calculated to be less than ±0.3 mm, not compromising the localization of the selected VOI within the hepatic parenchyma.

In order to quantify the HLC, water-unsuppressed spectra consisting of 32–52 scans were acquired with a T_E of 8 ms, a mixing time of 20 ms, a T_R of 6.5 s and 4096 complex points. The T_E of 8 ms was used to minimize unwanted gradient-induced sidebands to the water peak (30), which, although still visible, did not hamper accurate peak integration of both the water and visible lipid resonance at 1.3 ppm (Lip1.3). The T_2 relaxation times of water and Lip1.3 were estimated by acquiring spectra with different T_E values (5, 8, 10, 15, 20, 25, 30 and 35 ms) and fitting the peak area decay with a monoexponential function.

Intrahepatic metabolites were assessed by acquiring additional spectra from the same VOI with the same STEAM sequence, this time preceded by VAPOR water suppression and outer volume saturation modules (seven CHESS pulses of 25 000 μs) and including a 15 000 μs gauss pulse during the T_M period (28). These spectra consisted of 16 scans for phantoms and 86–128 scans for mice, and were acquired with a T_E of 2.8 ms, a mixing time of 20 ms, a T_R of 5 s and 2048 complex points. Since water suppression and outer volume saturation increase the total scan time, compensatory shortening of the acquisition time was achieved by decreasing the sampling points to 2048, in order to keep the total running time within one breathing cycle. To determine the T_2 of the fatty-acyl protons different T_E values were used (2.8, 7.2, 14.5, 21.7, 28.9 and 36.2 ms) and the signal decay fitted with a monoexponential function.

The acquisition of one water-unsuppressed spectrum for HLC quantification and one water-suppressed spectrum for fatty acid characterization was completed within approximately 20 min. The acquisition time is driven by the number of scans and the effective T_R, which is slightly longer than that programmed in the sequence due to respiration-triggering.

Tissue extraction and HR-NMR

Livers were lyophilized and pulverized to a fine powder and the lipids extracted with chloroform:methanol (2:1) following the method

originally developed by Folch (31). The aqueous phase containing hydrophilic metabolites was discarded and the chloroform phase containing the total lipids dried under nitrogen atmosphere to prevent possible oxidation. Lipid samples were dissolved in 500 μl of *d*-chloroform and pyrazin was used as internal standard for quantification. Fully relaxed ^{1}H-NMR spectra were acquired in a DRX-600 spectrometer (Bruker BioSpin, Fällanden, Switzerland) equipped with a cryoprobe tuned to ^{1}H. Spectra consisted of 16 scans and were obtained with a pulse–acquire sequence using a pulse delay of 10 s and an acquisition time of 2.5 s. The soybean oil-in-water emulsion was diluted in deuterated water and its fully relaxed ^{1}H-NMR spectrum was acquired with a pulse delay of 4 s, an acquisition time of 2.5 s and suppression of residual water.

^{1}H-MRS data and calculations

Individual spectra were corrected for B_0 drift and phase, summed together and analyzed by line fitting with LCModel version 6.3-1E (32) using SPTYPE liver-11 with automatic metabolite simulation. Lipid content was estimated from spectra acquired without water suppression as shown in Equation [1], in which $S(0)$Lip1.3 is the T_2-corrected peak area of Lip1.3 and is equal to $\frac{S(T_E)\text{Lip1.3}}{e^{-T_E/T_{2\,(\text{Lip1.3})}}}$, and $S(0)$water is the T_2-corrected peak area of water and is equal to $\frac{S(T_E)\text{water}}{e^{-T_E/T_{2\,(\text{water})}}}$.

$$\text{HLC}(\%) = \frac{S(0)\text{Lip1.3}}{S(0)\text{Lip1.3} + S(0)\text{water}} \times 100. \quad [1]$$

The chemical composition of the bulk of fatty-acyl chains in hepatic lipids, hereafter called fatty acid composition, was estimated from water-suppressed spectra acquired *in vivo* and also from HR-NMR spectra of liver tissue extracts, following the work of other authors (14,23,33) by using Equations [2]–[9] (see Fig. 1 for guidance). Since chemically similar protons are present in distinct fatty acids, the measured ^{1}H-MRS indices report a theoretical fatty-acyl chain representing an average of those in hepatic lipids. Briefly, in Equations [2]–[5], the area of each resonance was compared with that of the terminal methyl groups (Lip0.9) and normalized for the number of protons. In the equations, ndb is the number of double bonds, FA is fatty-acyl chains, PU is the number of poly-unsaturated bonds and UFA is unsaturated fatty-acyl chains. For sake of clarity, it should be noted that the saturation index estimated by Equation [2] depends not only on the saturation level of the chain but also on the chain length; in Equation [3], the possible contribution from glyceryl protons (Lip5.2) in the spectra acquired *in vivo* was assumed to be negligible; contributions from non-lipid protons with resonances in the same region as the fatty-acyl protons (e.g. lactate and alanine at 0.9–1.5 ppm; glutamate, glutamine, isoleucine at 2.0–2.2 ppm; aspartate at 2.8 ppm) were assumed to be negligible, given the molarity ratio between fatty-acyl protons and those from other metabolites (34,35).

$$\text{Saturation Index} = \frac{\text{Lip1.3}\times 3}{\text{Lip0.9}\times 2} \quad [2]$$

$$\text{ndb} = \frac{\text{Lip5.3}\times 3}{\text{Lip0.9}\times 2} \quad [3]$$

$$\text{PU/FA(or PUFA)} = \frac{\text{Lip2.8}\times 3}{\text{Lip0.9}\times 2} \quad [4]$$

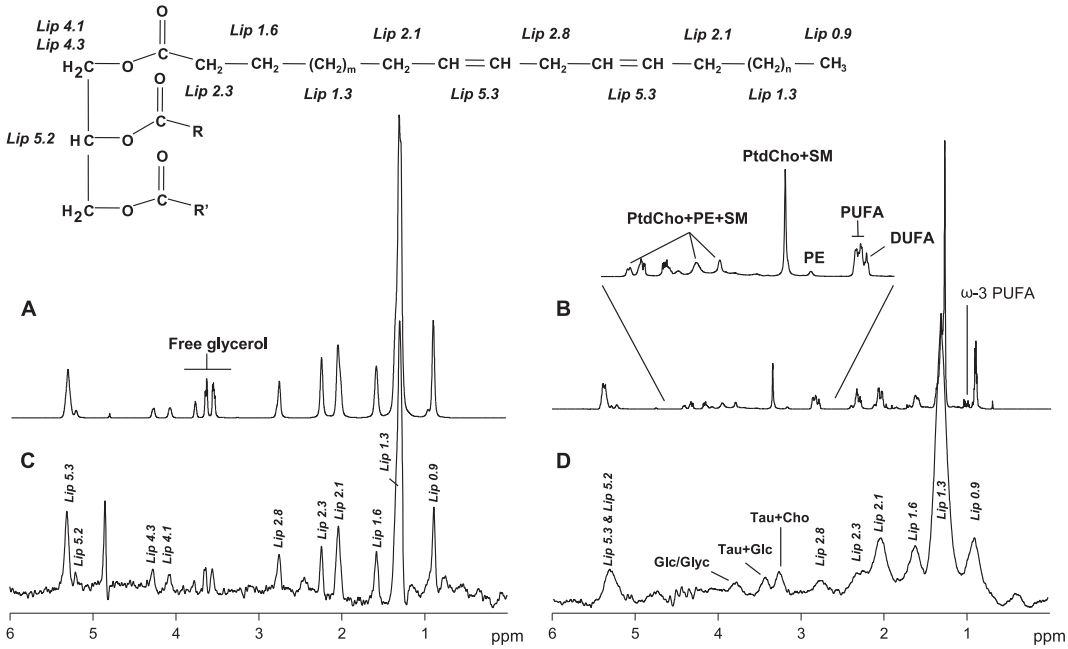

Figure 1. Identification of the different types of proton in the fatty-acyl chains by their specific resonances in the ^{1}H-MR spectrum. Top, the general structure of a glyceride where the protons are labeled according to their chemical shift. In triglycerides both R and R′ are additional fatty-acyl chains. In phospholipids R′ is a phosphate group attached to a simple molecule (e.g. choline in PtdCho). Spectra were obtained by HR-NMR performed in a soybean oil-in-water emulsion (A) and in lipid samples extracted from the mouse liver (B); and by ^{1}H-MRS with ultra-short T_E STEAM performed in a phantom from soybean oil-in-water emulsion (C) and in the mouse liver (D) *in vivo*. In addition to glycerides, the soybean oil sample also contained free glycerol, whose protons are identified in (A). The inset in (B) depicts specific resonances from membrane phospholipids visible in the HR-MR spectrum of the liver extracts. Specific resonances from poly-unsaturated (PUFA) and di-unsaturated (DUFA) fatty-acyl chains are also identified. Cho, choline-containing compounds; Glc/Gly, glucose/glycogen; PE, phosphatidylethanolamine; PtdCho, phosphatidylcholine; SM, sphingomyelin; Tau, taurine.

$$\mathrm{UFA}(\%) = \frac{\mathrm{Lip2.1}\times 3}{\mathrm{Lip0.9}\times 4}\times 100. \quad [5]$$

Fatty-acyl chains can either be saturated (SFA) or unsaturated (UFA), yielding UFA(%) + SFA(%) = 100 (Equation [6]). Equation [4] yields the contribution of PUFA in the case where no more than one Lip2.8 group exists per chain, i.e. the fatty-acyl chains may contain either zero, one or two double bonds. This is a fair approximation for hepatic cytosolic lipids (mainly triglycerides), since the presence of three or more conjugated double bonds is minimal in hepatic triglycerides in mice fed a standard chow diet (36). Under such circumstances, MUFA(%) + PUFA(%) + SFA(%) = 100 (13), and the content of MUFA can be determined as shown in Equation [7].

$$\mathrm{SFA} = 100 - \mathrm{UFA} \quad [6]$$

$$\mathrm{MUFA} = \mathrm{UFA} - \mathrm{PUFA}. \quad [7]$$

The mean number of poly-unsaturated bonds per UFA was used as an index of the poly-unsaturation degree and estimated as the area of the bisallylic protons (Lip2.8) relative to that of the allylic ones (Lip2.1) using the following equation.

$$\mathrm{PU/UFA} = \frac{\mathrm{Lip2.8}\times 2}{\mathrm{Lip2.1}}. \quad [8]$$

The mean chain length (MCL) was estimated as shown in Equation [9]. One carbon for the terminal methyl group (Lip0.9), one for the carboxylic group, one for Lip2.3 and finally another for Lip1.6 was assumed for each chain, accounting for the term 4. The number of carbons from the other fatty-acyl groups varies with chain length and unsaturation degree. Their areas in the ^{1}H MR spectrum were normalized to the terminal methyl group with weightings for the carbon to proton ratio.

$$\mathrm{MCL} = \frac{{}^1/_2(\mathrm{Lip1.3} + \mathrm{Lip2.1} + \mathrm{Lip2.8}) + \mathrm{Lip5.3\&5.2}}{{}^1/_3\times\mathrm{Lip0.9}} + 4 \quad [9]$$

Statistics

Numeric data are expressed as mean ± SEM. Statistical difference was accepted for $P < 0.05$ as determined with a paired or unpaired two tailed Student *t* test, or with a one way ANOVA with a Newman–Keuls post-test when comparing more than two data sets. A repeated measurement one way ANOVA with Newman–Keuls post-test was used to test statistical significance of changes in the measured parameters following STZ injection.

RESULTS

Method validation in phantoms

In order to validate the ^{1}H-MRS method for HLC quantification *in vivo*, we first performed studies in phantoms prepared from a soybean oil-in-water emulsion, with lipid contents ranging from 0 to 20%. The lipid content was calculated from spectra acquired without water suppression (Fig. 2(A)). In these spectra, the bulk of fatty-acyl methylene protons (Lip1.3) was clearly identified and quantified in all standards, while other resonances were not as prominent, especially in the low lipid content emulsions. The T_2 both of the water protons and of Lip1.3 decreased with increasing lipid content (Table 1). The lipid content as calculated by ^{1}H-MRS was in excellent correlation (Pearson $r = 0.997$, $P < 0.0001$) with the known lipid content of the diluted standards (Fig. 2(B)).

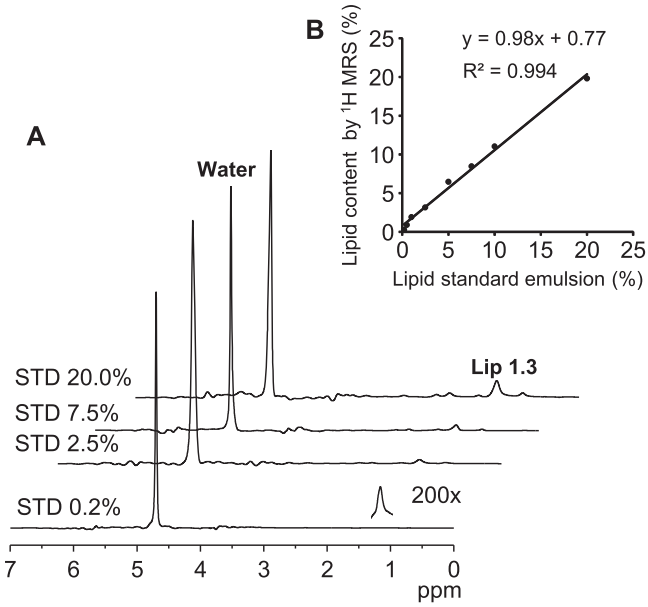

Figure 2. Validation of the ^{1}H-MRS quantification method on a phantom. (A) ^{1}H-MR spectra acquired with STEAM from (2 × 2 × 2) mm^3 volumes in soybean oil emulsions. The water resonance at 4.7 ppm and the main lipid resonance at 1.3 ppm are identified. Lipid contents of 0.2, 2.5, 7.5 and 20% are shown as examples. (B) Linear relation between the ^{1}H-MRS measurements and the known lipid content of the soybean oil emulsion standards.

Suppression of the water signal in the ^{1}H-MRS acquisitions in the soybean oil-in-water emulsion resulted in the clear identification of all the fatty-acyl proton resonances (Fig. 1(C)). The T_2 values of the different types of proton in the 20% oil-in-water emulsion ranged from 12 to 19 ms (Table 2). A typical spectrum acquired with 2.8 ms T_E STEAM is shown in Fig. 1(C); as can be appreciated, it closely resembles that obtained from the same lipid emulsion by HR-NMR *in vitro* (Fig. 1(A)). The two types of spectroscopy experiment yielded comparable values for the

Table 1. T_2 relaxation times of the water and the methylene protons of the fatty-acyl chains (Lip1.3) determined by monoexponential fit of the peak areas with increasing echo time from the ^{1}H-MR spectra acquired in a lipid emulsion phantom with STEAM without water suppression. The different standards were prepared by dilution of a 20% soybean oil emulsion in distilled water

Lipid content of the standard emulsion		0%	0.2%	0.5%	1%	2.5%	5%	7.5%	10%	20%
T_2 (ms)	Water	416	345	345	333	300	236	187	169	152
	Lip1.3	–	29	29	27	29	21	23	18	17

Table 2. T_2 relaxation times (ms) of the fatty-acyl protons (identified by their chemical shift, see also Fig. 1) determined by monoexponential fit of the peak areas with increasing echo time from the ^{1}H-MR spectra acquired with STEAM and water suppression. There were no significant differences between the T_2 values of the several lipid resonances, either within the phantom measurements (20% oil-in-water lipid emulsion) or within the mouse liver measurements (one way ANOVA with Newman–Keuls post-test)

	Soybean emulsion (N = 3)	Mouse liver (N = 4–5)
Lip0.9	19 ± 1	19 ± 2
Lip1.3	16 ± 1	23 ± 3
Lip1.6	12 ± 1	17 ± 1
Lip2.1	18 ± 3	18 ± 3
Lip2.3	19 ± 1	21 ± 5
Lip2.8	16 ± 2	17 ± 4
Lip5.3	16 ± 2	23 ± 5

indices used to characterize the fatty-acyl chains (Table 3). We further assessed the method's response to changes in the saturation profile in mixtures prepared from SO and PO. The MCL of the fatty-acyl chains in SO was 17.14 by ^{1}H-MRS and 17.78 by HR-NMR, similar to that found in PO: 17.70 by ^{1}H-MRS and 17.98 by HR-NMR. These oils had similar UFA contents, as determined by HR-NMR (SO, 87%; PO, 82%) and ^{1}H-MRS (SO, 85%; PO, 84%), but distinct contributions from PUFA and MUFA (Fig. 3). When SO:PO mixtures were studied, indices related to the unsaturation degree reflected the relative contributions of each oil (Fig. 3), supporting the applicability of those indices to detect changes in fatty acid saturation *in vivo*. Nevertheless, ^{1}H-MRS analysis underestimated ndb relative to HR-NMR by, on average, 13%. This discrepancy could be explained by the chemical shift error between Lip0.9 and Lip5.3, in the presence of the inhomogeneous sensitivity of the surface coil used.

MRS of the mouse liver

To place the VOI for *in vivo* ^{1}H-MRS avoiding major blood vessels, MR images were acquired from the abdominal region, yielding well-defined anatomical information (Fig. 4(A)). The line width at half maximum signal height for the water peak was 69 ± 1 Hz. Hepatic water T_2 relaxation time was 8.0 ± 0.3 ms and that of Lip1.3 was 19 ± 1 ms, as determined from spectra acquired without water suppression. The HLC determined by ^{1}H-MRS was in excellent correlation (Pearson r = 0.959, $P < 0.0001$) with that determined *in vitro* in liver tissue extracts (Fig. 3(C)). Hepatic water content, as measured in a subset of mice, was 70% m/m, which is equivalent to about 39 M, making the approximation that liver tissue density is 1000 g/L. For an HLC of 1% *in vivo* (lower limit of the observed values), the bulk of fatty-acyl methylene protons roughly represents 1% of those of water, thus existing in a concentration of about 390 μmol per gram of wet weight or about 1325 μmol per gram of dry weight (experimental conversion factor of 3.4). Since about seven methylene groups exist, on average, in a fatty-acyl chain (Table 3), the approximate concentration of fatty-acyl chains in the liver would be about 190 μmol per gram of dry weight, below the minimum value measured in the liver extracts (280 μmol per gram of dry weight). The HLC of the studied mice ranged from 1.1 to 6.9% and was correlated (Pearson r = 0.909,

Table 3. Characterization of hepatic fatty-acyl chains by ^{1}H-MRS *in vivo* and by HR-NMR *in vitro* in the soybean oil-in-water emulsion phantom and in the mouse liver

	Saturation index	ndb	PU/FA or PUFA	PU/UFA	UFA	SFA	MUFA	MCL
	Eq. [3]	Eq. [4]	Eq. [5]	Eq. [8]	Eq. [6]	Eq. [7]		Eq. [9]
Soybean oil-in-water emulsion phantom								
^{1}H-MRS (N = 3)	9.20 ± 0.40	1.25 ± 0.23	0.66 ± 0.03	0.88 ± 0.07	76 ± 7%	24 ± 7%		17.88 ± 1.55
HR-NMR	9.02	1.53	0.67	0.76	86	14	NA	17.88
Mouse liver (control)								
^{1}H-MRS	7.34 ± 0.16	0.92 ± 0.09	0.42 ± 0.07	0.53 ± 0.08	80 ± 5%	20 ± 5%	38 ± 7%	15.20 ± 0.44
HR-NMR	8.71 ± 0.17*	1.56 ± 0.01*	0.85 ± 0.08*	1.39 ± 0.03**	61 ± 1%*	39 ± 1%*	NA	17.91 ± 0.20*
Mouse liver (14days after STZ injection)								
MRS	6.46 ± 0.16	0.78 ± 0.09	0.17 ± 0.05	0.29 ± 0.07	55 ± 6%	45 ± 6%	38 ± 2%	13.32 ± 0.26
HR-NMR	7.8 ± 0.13**,§	1.37 ± 0.02**,§§	0.86 ± 0.04***	1.67 ± 0.06***,§	52 ± 1%§§	48 ± 1%§§	NA	16.44 ± 0.17***,§§

*$P < 0.05$,
**$P < 0.01$ and
***$P < 0.001$ versus ^{1}H-MRS *in vivo* for the same group determined with paired two tailed Student t tests.
§$P < 0.01$ and
§§$P < 0.001$ versus HR-NMR in control mice determined with unpaired two tailed Student t tests. NA, not applicable due to the presence of tri- and higher unsaturations

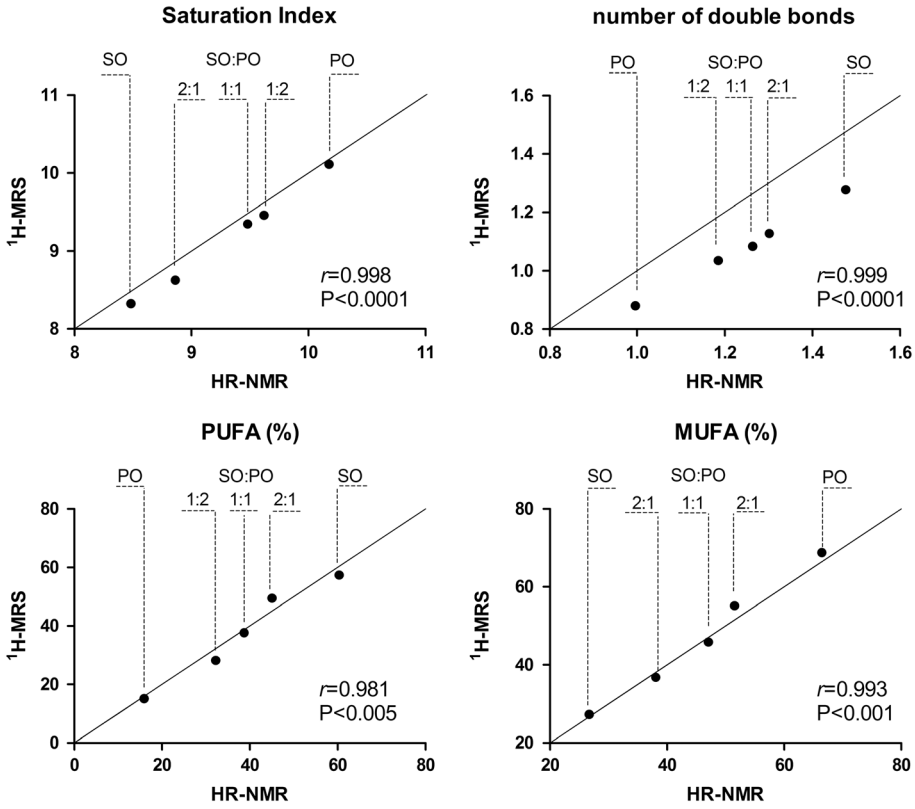

Figure 3. Saturation index, mean ndb, PUFA and MUFA estimated from spectra acquired by ^{1}H-MRS with ultra-short T_E STEAM and by HR-NMR in SO, PO and respective mixtures. The identity line and Pearson correlation values between methods are also shown for each plot.

$P < 0.0001$) with their body weight (Fig. 3(D)). Mice were studied at different ages, with older animals (7–10 months) displaying higher body weight than younger ones (4 months), as expected. The highest values for body weight and HLC were observed for mice of 7 months of age, with both younger and older mice showing lower body weights and HLC.

The group of mice used to investigate the hepatic fatty acid composition both by ^{1}H-MRS *in vivo* and HR-MR *in vitro* showed an HLC of 1.4 ± 0.1%. Seven fatty-acyl resonances could be identified in spectra acquired *in vivo*, but, compared to the phantom measurements, Lip4.1 and Lip4.3 from the glyceryl moiety of triglycerides were not clearly discernible (Fig. 1(D)). In addition, other hepatic resonances were detected and tentative assignments were made for taurine (3.2 and 3.4 ppm), choline containing compounds (3.2 ppm), glucose (3.4 and 3.8 ppm) and glycogen (3.8 ppm), based on previous ^{1}H-MRS observations *in vivo* in humans (37) and HR-MAS measurements made in liver samples from humans and rodents (38–41). The T_2 of the fatty-acyl resonances ranged from 17 to 23 ms (Table 2), in the same range as that determined in the phantom. The fatty acid composition assessed by ^{1}H-MRS *in vivo* was distinct from that obtained by HR-NMR in liver extracts *in vitro*. The percent UFA was higher in the measurements made *in vivo*; nevertheless, parameters related to the unsaturation degree of the fatty-acyl chains (ndb, PU/FA – poly-unsaturated bonds per fatty-acyl chain – and PU/UFA – poly-unsaturated bonds per unsaturated fatty acyl chain) were higher when estimated from the HR-NMR spectra (Table 3). The MCL was also longer in the latter case, in agreement with higher saturation indices measured from HR-NMR spectra. Several resonances attributed to phospholipids were visible in the HR-NMR spectra of liver extracts (Fig. 1(B), inset). The terminal methyl group of ω-3 PUFA was also clearly visible in those spectra. This resonance is shifted downfield relative to the other methyl groups and represented 12 ± 1% of the total Lip0.9. In addition, in the HR-NMR spectra, PUFAs with three or more double bonds were resolved from di-unsaturated fatty-acyl chains by the downfield shift of bis-allylic protons at 2.8 ppm (Lip2.8).

Effect of STZ on HLC and fatty acid composition

To evaluate the impact of a metabolic stress on the HLC and fatty acid composition, we studied STZ-induced diabetic mice. The HLC of these mice determined by ^{1}H-MRS *in vivo* before STZ injection was 1.7 ± 0.3%, similar to that determined in the cohort of mice used for the hepatic lipid profile study, but decreased to 0.6 ± 0.04% ($P < 0.05$) 7 days post-STZ injection, without further changes until the end of the study (0.7 ± 0.1% 14 days post-STZ, $P < 0.05$ versus before STZ). The indices used to characterize hepatic fatty-acyl chains in mice before STZ administration were not statistically different from those estimated for the cohort of control mice (Table 3 and Fig. 5). Progressive alterations in the composition of hepatic fatty acids were detected in the longitudinal follow-up of STZ-induced diabetic mice by ^{1}H-MRS *in vivo*. Figure 5 shows the region from 0.6 to 2.6 ppm for representative liver spectra acquired before STZ administration and 14 days afterwards. As can be appreciated, after STZ injection, signals from methylene (Lip1.3) and allylic (Lip2.1) protons were decreased relative to the terminal methyl group (Lip0.9). These spectral observations translated into significant alterations of the measured indices. Shorter fatty-acyl chains were already detected 7 days post-STZ injection along with a tendency for lower saturation

NMR IN BIOMEDICINE

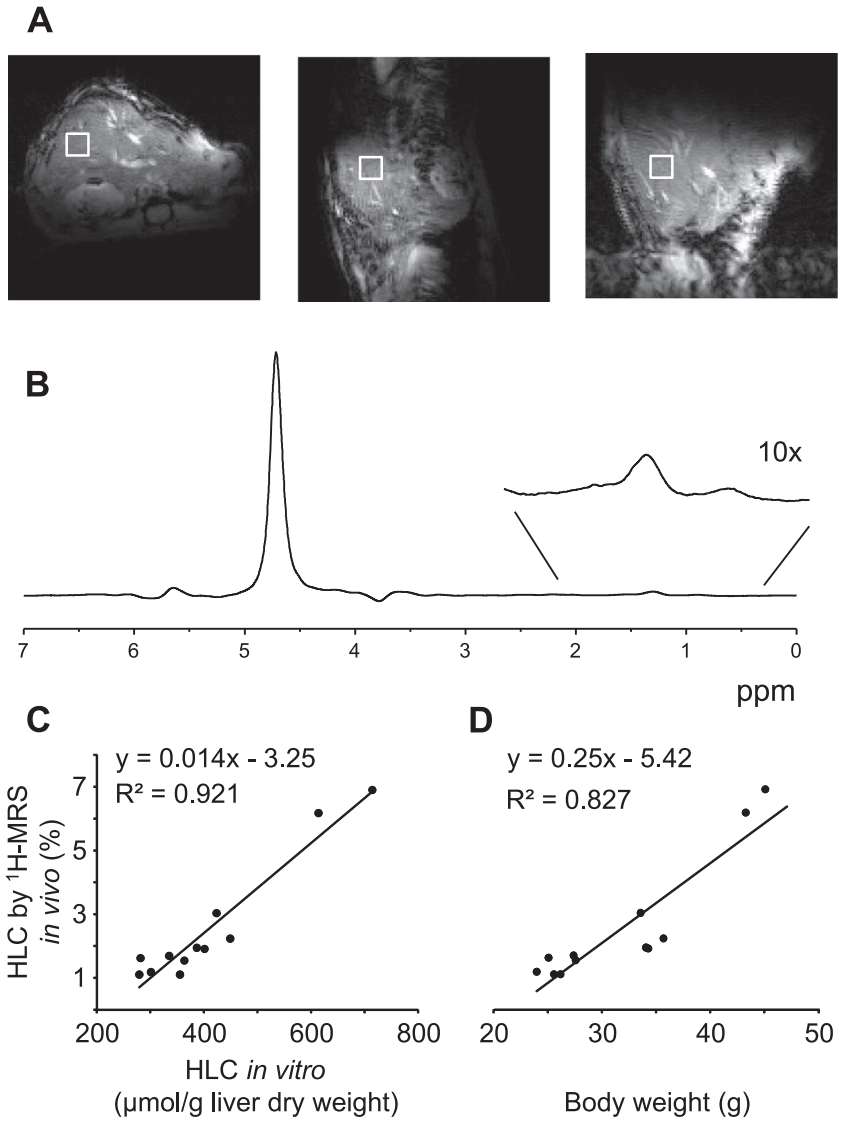

Figure 4. *In vivo* MRI and ^{1}H-MRS of the mouse liver. (A) Gradient echo anatomical images acquired from the abdominal region of a mouse in the sagittal, axial and coronal orientations; minimum T_R/T_E provided good contrast for the identification of the blood vessels. A typical VOI of (2 × 2 × 2) mm^3 is also represented in the images. (B) Representative spectrum acquired with STEAM from the depicted volume showing the water resonance at 4.7 ppm and the resonance from the main lipid component at 1.3 ppm. (C) Linear relation between the HLC determined in mice by ^{1}H-MRS *in vivo* and that determined in the liver tissue extracts by HR-NMR. (D) Linear relation between the HLC and the body weight of the mice.

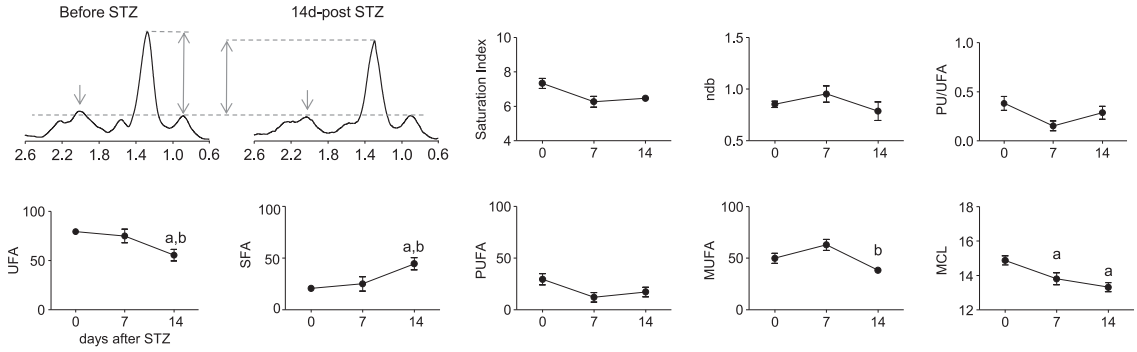

Figure 5. Spectroscopic alterations (grey arrows and dotted lines) in the 0.6–2.6 ppm region observed by ^{1}H-MRS *in vivo* in the liver of mice 14 days after the injection of STZ. Temporal evolution of the fatty acid composition after the injection of STZ is shown in the graphs. [a] $P < 0.05$ versus before STZ injection. [b] $P < 0.05$ versus 7 days STZ determined with repeated measures one way ANOVA and Newman–Keuls post-test.

index ($P = 0.07$). By day 14, the contribution of SFA to hepatic fatty-acyl chains was more than twice that observed before STZ injection. Lower unsaturation was ascribed to a reduction of both hepatic MUFA and PUFA. The MUFA-to-SFA ratio was 2.6 ± 0.4 before STZ injection and decreased to 2.0 ± 0.4, 7 days after STZ injection ($P < 0.05$) and further to 0.9 ± 0.2 by day 14 post-STZ ($P < 0.01$ versus before STZ and $P < 0.05$ versus 7 days post-STZ). The PUFA-to-SFA ratio decreased from 1.6 ± 0.4 before STZ injection to 0.3 ± 0.1 by day 7 post-STZ ($P < 0.05$), with no further changes by day 14 post-STZ (0.5 ± 0.2, $P < 0.05$ versus before STZ).

HR-NMR analyses of liver extracts 14 days post-STZ injection reported longer chains, higher saturation index and more double bonds and poly-unsaturated bonds per chain relative to the matched assessments by ^{1}H-MRS *in vivo* (Table 3), reproducing the observations in the control cohort. However, unlike the case in controls, the UFA-to-SFA ratio was similar in both the *in vivo* and *in vitro* measurements in STZ mice. This is because this ratio was already unbalanced towards SFA in the fatty-acyl chains detected *in vivo*. Compared with findings in liver extracts from control mice, in STZ mice HR-NMR reported shorter chains and saturation indices with a greater contribution from SFA, but at the same time more PU/UFA (Table 3).

DISCUSSION

We employed ^{1}H-MRS *in vivo* at 14.1 T to study an 8 μl volume of the mouse liver, with particular focus on resonances from protons in the fatty-acyl chains of hepatic lipids. We were able to follow alterations in the composition of the fatty-acyl chains, even for reduced hepatic lipid levels, i.e. after the induction of type 1 diabetes by STZ injection. In addition to the dominating resonances from the fatty-acyl protons, we also document the presence of other metabolites, notably choline containing compounds, taurine and glucose and/or glycogen (Fig. 1(D)), similarly to previous observations in human studies *in vivo* (37). Since those resonances include contributions from several molecules, further studies are envisaged in order to unequivocally identify non-lipid metabolites in the mouse liver by ^{1}H-MRS *in vivo*.

Estimations of fatty acid composition by ^{1}H-MRS are based on resonances from protons that can be part of the molecular structure of different lipid classes, each one including several species varying in the length and saturation of their hydrocarbon chains. Analyses by ^{1}H-MRS lack the power to resolve the lipid classes and species to which the observed fatty-acyl protons belong. A comprehensive lipid profile may be achieved by sophisticated analyses using data from mass-spectrometry measurements made after subjecting biological samples to a chromatography separation (42–44). While such methods necessarily demand tissue harvesting, ^{1}H-MRS *in vivo* has the advantage of allowing non-invasive assessments and, furthermore, its estimations are in good correlation with gas chromatography data (45). Therefore, although reporting a theoretical fatty-acyl chain averaged across multiple species, ^{1}H-MRS *in vivo* remains a relevant methodology in the scope of hepatic lipid abnormalities, especially in humans (15,39), but also in rodent models (23,25,45–47), given that repeated measurements may be made in longitudinal studies to assess disease progression and/or treatment outcome. The most abundant lipid classes in the liver of mice are triglycerides and phospholipids (10,36,48). Phospholipids are important components of biological membranes, whereas triglycerides constitute over 95% of the lipid cytosolic droplets (43). Due to their reduced mobility, membrane phospholipids are invisible by ^{1}H-MRS *in vivo* (49). Thus, it is reasonable to assume that fatty-acyl resonances observed *in vivo* mainly report chains in mobile cytosolic triglycerides, which constitute important metabolic fuels. Conversely, during the liver extraction procedure, structural lipids from membranes are released to the organic medium, thus being detected in subsequent HR-NMR measurements and, as we show and discuss further, strongly contributing to the spectra acquired *in vitro*.

In addition to the biochemical concerns discussed above, specific technical aspects should also be addressed. In mouse liver spectroscopy, in order to avoid contamination from high caliber blood vessels, abdominal fat or neighboring organs such as the gallbladder, a careful placement of the voxel confined to the hepatic parenchyma is critical. At high magnetic fields, the possibility to achieve ultra-short T_E values is highly beneficial to study microliter volumes (28,50). Therefore, we used a VOI size of (2 × 2 × 2) mm^3, while most studies use larger volumes to increase the SNR (17,23–25,27), with a concomitant higher risk of contamination from extra-hepatic structures. Quantification of HLC and characterization of fatty acids by ^{1}H-MRS *in vivo* rely on the comparison of peak areas from different resonances and particular characteristics of the protons contributing to each resonance in the living organ need to be considered. T_1 relaxation confounding effects were overcome by using T_R values of 6.5 s (water-unsuppressed spectra) and 5 s (water-suppressed spectra), which allowed full recovery of *z*-magnetization for the water and fatty-acyl protons, respectively. As in other studies (13,25,45,46), T_2 relaxation times were estimated with a monoexponential function, which overlooks *J*-coupling effects on the signal decay of the fatty-acyl protons (16,51,52). Nonetheless, in a study where spectra were acquired with STEAM from the liver of healthy volunteers (52), accounting for *J*-coupling modulation yielded T_2 values comparable to those obtained from the simplified monoexponential model, supporting the accuracy of our T_2 estimations. Hepatic water T_2 was 8 ms, shorter than that reported for mice at 11.7 (53), 9.4 (27) and 7 T (25). T_2 shortening with increasing magnetic field strength has been previously observed for brain metabolites (54). Given the fast relaxation of the water protons, notably relative to the methylene ones, T_2 corrections were applied for quantitative estimations of HLC. The T_2 values of the fatty-acyl protons ranged from 17 to 23 ms, also shorter than previous observations with PRESS at 9.4 T (27) but in the range of the values observed in another study with PRESS at 7 T (25). With a 2.8 ms T_E, T_2 differences yield an error below 5% when comparing peak areas from fatty-acyl protons, while *J*-coupling (J_{AX} of 7 Hz, typical for the fatty-acyl protons) should contribute as little as 0.01% to the signal loss according to $\cos(\pi T_E J_{AX})$. Therefore, corrections for signal losses due to T_2 and *J*-coupling were dispensed as further corroborated by the phantom experiments (Table 3). The T_2 values of the fatty-acyl protons in the soybean oil-in-water emulsion (12–19 ms) were comparable to those observed in the mouse liver *in vivo* and shorter than those reported for pure oils (25,51,52), which is relevant for validation of the method, and further supports the accuracy of our results in the mouse liver *in vivo*. Moreover, changes in the saturation degree of the fatty-acyl chains could be successfully identified by ^{1}H-MRS in mixtures prepared from SO (high levels of PUFA) and PO (high levels of MUFA), demonstrating the applicability of the method to follow alterations of the hepatic fatty acid composition *in vivo*.

It was interesting to observe a relatively wide range of HLC in control mice in our studies: from 1 to 7% (Fig. 3(C)). The upper limit of the measured range of values is lower than the 10–30% HLC reported for models of steatosis (18,23,24), yet it is comparable to that found in mice fed a high fructose diet, inducing hepatic lipid accumulation to a value of about 8% (26). We observed that mice showing abnormally high HLC were somewhat overweight when compared with the average of their counterparts, but not necessarily older. In fact, a good correlation was found between the HLC and the body weight of mice (Fig. 4(D)). Our findings show that hepatic lipid accumulation to levels similar to those induced by lipogenic diets may take place even with a standard chow diet in parallel with the development of obesity, independently of aging-associated weight gain. It would be of interest to follow up these preliminary observations in future studies.

Fatty-acyl chains in hepatic triglycerides may originate from dietary lipids or be synthesized *de novo*. In our experiments, dietary fat derived from soybean oil that is composed mainly of triglycerides from unsaturated 18-carbon fatty acids with up to a 20% contribution from saturated 16- and 18-carbon fatty acids (55,56), in agreement with the fatty acid composition estimated in the soybean oil-in-water emulsion (Table 3). On the other hand, *de novo* lipogenesis culminates with the synthesis of 16-carbon saturated palmitoyl-CoA, which can be further elongated or desaturated by specific hepatic enzymes. We estimate an MCL of 15 carbons for cytosolic fatty acids in control mice, similar to previous findings using ^{1}H-MRS *in vivo* (27). Since this value represents an average of the ensemble of fatty-acyl chains, it is indicative of the presence of both shorter and longer chains. Chains shorter than 16 carbons necessarily denote the presence of partially catabolized species in healthy mice. Comparatively, hepatic fatty-acyl chains in steatotic mice are, on average, longer than 18 carbons (46,57), in part due to increased anabolic fatty acid elongation, at least in mice fed a high fat diet (57). On the other hand, in mice that experienced a reduction of HLC following the injection of STZ, we observed a reduction of the MCL, which could reflect increased fatty acid catabolism (6). Regarding the saturation profile, about 80% of the fatty-acyl chains in the liver of control mice were UFA (with equal contributions from PUFA and MUFA), in agreement with other ^{1}H-MRS studies in healthy control mice (25,27). We also found that, on average, hepatic fatty-acyl chains had one double bond and a saturation index of about 7. However, it is likely that the ndb reported by ^{1}H-MRS is slightly underestimated, as suggested by the findings in oil phantoms (Fig. 3). Using the same indices, Ye *et al*. (27) report similar values: about 1.2 and about 7, respectively. On the other hand, Ramamonjisoa *et al*. (25) found that the mean ndb in hepatic lipids was about 1.7 and the saturation index about 10. The younger age of the mice in our study (4 months) and in that of Ye *et al*. (6 months) may explain the different findings relative to the study of Ramamonjisoa *et al*., performed in mice about 10 months old. Taken together, these studies suggest that the composition of hepatic fatty-acyl chains in mice may exhibit age-related variations, even in the absence of lipid-modulating interventions, and, in principle, this evolution could be monitored by ^{1}H-MRS methods. The aforementioned alterations in HLC and MCL of STZ-induced diabetic mice were also accompanied by noticeable changes in fatty acid saturation. Notably, we observed a reduction of the MUFA-to-SFA ratio, which could be related to the absence of insulin-stimulated stearoyl-CoA desaturase activity, synthesizing MUFA from SFA precursors (58,59). On the other hand, fatty-acyl chains with low unsaturation have also been observed in high fat diet models that lead to hepatic lipid accumulation (47). In this case, however, this likely results from the accumulation of dietary saturated lipids, and obscures alterations in lipid metabolism that would lead to increased MUFA due to augmented stearoyl-CoA desaturase activity (57). Hence, changes in the hepatic fatty acid saturation parameters determined by ^{1}H-MRS *in vivo* may be indicative of diverse metabolic imbalances and should be carefully interpreted with respect to the phenotype.

We complemented ^{1}H-MRS *in vivo* with HR-NMR assessments in liver extracts, which also detected fatty-acyl protons from membrane lipids, mostly phospholipids (60). In fact, HR-NMR estimations of fatty acid composition were strongly driven by the presence of these species, which can represent over one-half of the lipids extracted from the liver of mice (10,36). For example, SFA accounted for ~20% of the hepatic cytosolic chains (assessed by ^{1}H-MRS *in vivo*), but had a significantly higher contribution (~40%) in the liver extracts. Assuming that 50% of the lipids in the extracts derive from membranes (36) and that half of these are saturated (61), 25% of the fatty-acyl chains in total lipids would derive from membrane SFA and 10% from cytosolic SFA. Hence, in total, SFA would contribute to 35% of the fatty-acyl chains in the liver extracts, in good agreement with our estimations by HR-NMR. Relative to ^{1}H-MRS *in vivo*, HR-NMR estimations reported higher PU/UFA and longer MCL. These differences further demonstrate the presence of membrane lipids, which, compared to cytosolic triglycerides, are composed of longer fatty-acyl chains with a higher degree of polyunsaturation (62,63). Notably, PUFAs with three or more methylene interrupted double bonds were identified in liver extracts by the downfield shift of Lip2.8 resonance. These same trends were reported by other authors when adipose tissue lipids were assessed in the extracted tissue by HR-NMR relative to ^{1}H-MRS measurements *in vivo* (64). Phosphatidylcholines (PtdCho) account for at least one-half of membrane phospholipids, and the second most abundant class is that of phosphatidylethanolamines (36,65). It can be assumed that the singlet at 3.32 ppm in the HR-NMR spectra is almost exclusively due to PtdCho, since levels of sphingomyelin, another choline-containing membrane lipid, are comparatively very small in the liver (48,65–67). This approximation yields that ~30%[†] of the fatty-acyl chains can be ascribed to PtdCho in total hepatic lipids of control mice. This contribution would be only about 13% for the overweight mice in our study, in line with a higher contribution from cytosolic lipids in this case, as supported by higher HLC detected by ^{1}H-MRS *in vivo*. On the other hand, the contribution of PtdCho to the fatty-acyl chains in the liver extracts from STZ-induced diabetic mice would be about 32% and not higher than that of control mice, as would have been expected due to a zreduced contribution from cytosolic lipids (lower HLC by ^{1}H-MRS *in vivo*). This finding may reflect alterations in hepatic membrane lipids in these mice. Indeed, in rats, STZ administration has been shown to cause a depletion of all phospholipid classes (68).

[†]PtdCho contains three methyl groups in the choline residue and two terminal methyl groups from the fatty-acyl chains; its contribution to the total fatty acids in the extracts can be estimated as $\text{PtdCho}(\%) = \frac{\text{PtdCho}}{\text{Lip0.9}} \times \frac{2}{3} \times 100$, in which PtdCho is the area of the peak at 3.32 ppm.

In addition to possible alterations in PtCho levels, we observed significant changes in the fatty acid composition of total lipids in livers from STZ-induce diabetic mice, relative to control mice. Namely, we detected shorter fatty-acyl chains and a higher contribution from SFA, similarly to the findings for the cytosolic fatty-acyl chains in the ^{1}H-MRS studies *in vivo*, and suggesting concomitant alterations in the fatty acids from membrane lipids. Concordant with our findings, it has been shown that the contribution of SFA to liver phospholipids is increased in STZ-induced diabetes, supported by higher abundance of 16:0 chains (11,69). We also found the poly-unsaturation degree of the fatty-acyl chains in total lipids to be higher in livers from STZ mice when compared with controls. This could potentially be explained by the reduced contribution of cytosolic lipids in STZ mice with a concomitant increase in the relative abundance of PUFA from membrane species. In addition, higher PU/UFA could reflect alterations in the fatty acid profile of membrane lipids. Imbalances in PUFA in STZ-induced diabetes have previously been reported in liver phospholipids (11,69). Membrane phospholipids are important sources of precursors further metabolized in microsomes to bioactive compounds. For example, eicosanoids derived from arachidonic acid (20:4*n*-6) or docosahexaenoic acid (22:6*n*-3) have pro- and anti-inflammatory properties, respectively, and are able to regulate hepatic gene expression, including enzymes involved in lipid metabolism, which is relevant for the pathology of diabetes (11). Detailed insight into membrane species would require further analytical processing of hepatic lipid samples. While the scope of this study was to investigate alterations by ^{1}H-MRS *in vivo* under reduced HLC, a comprehensive overview of alterations in metabolic and regulatory lipid species would benefit from complementary lipidomics analyses and measurements of metabolic pathways.

CONCLUSION

We conclude that ^{1}H-MRS with an ultra-short T_E STEAM provides an important insight into the composition of the hepatic fatty-acyl chains in mice *in vivo*, even when they experience a reduction of their HLC. By combining data from *in vivo* and *in vitro* measurements we demonstrate that both the cytosolic triglycerides and membrane phospholipids from the livers of STZ-induced diabetic mice are enriched with shorter, SFA chains. Despite inherent analytical limitations, ^{1}H-MRS *in vivo* is a valuable method to follow modulation of hepatic fatty acids in the context of lipid-lowering interventions.

Acknowledgements

We thank Dr Daniel Gallichan for kindly proof-reading the manuscript and acknowledge support from the Centre d'Imagerie BioMédicale (CIBM) of the UNIL, UNIGE, HUG, CHUV, EPFL and the Leenaards and Louis-Jeantet Foundations.

REFERENCES

1. Tessari P, Coracina A, Cosma A, Tiengo A. Hepatic lipid metabolism and non-alcoholic fatty liver disease. Nutr. Metab. Cardiovasc. Dis. 2009; 19: 291–302.
2. Cohen JC, Horton JD, Hobbs HH. Human fatty liver disease: old questions and new insights. Science 2011; 332: 1519–1523.
3. Kotronen A, Vehkavaara S, Seppälä-Lindroos A, Bergholm R, Yki-Järvinen H. Effect of liver fat on insulin clearance. Am. J. Physiol. Endocrinol. Metab. 2007; 293: E1709–E1715.
4. Stefan N, Häring H-U. The metabolically benign and malignant fatty liver. Diabetes 2011; 60: 2011–2017.
5. Stephenson MC, Leverton E, Khoo EYH, Poucher SM, Johansson L, Lockton JA, Eriksson JW, Mansell P, Morris PG, MacDonald IA. Variability in fasting lipid and glycogen contents in hepatic and skeletal muscle tissue in subjects with and without type 2 diabetes: a ^{1}H and ^{13}C MRS study. NMR Biomed. 2013; 26: 1518–1526.
6. Jourdan T, Djaouti L, Demizieux L, Gresti J, Verges B, Degrace P. Liver carbohydrate and lipid metabolism of insulin-deficient mice is altered by trans-10, cis-12 conjugated linoleic acid. J. Nutr. 2009; 139: 1901–1907.
7. Haeusler RA, Han S, Accili D. Hepatic FoxO1 ablation exacerbates lipid abnormalities during hyperglycemia. J. Biol. Chem. 2010; 285: 26861–26868.
8. Araya J, Rodrigo R, Videla LA, Thielemann L, Orellana M, Pettinelli P, Poniachik J. Increase in long-chain polyunsaturated fatty acid n - 6/n - 3 ratio in relation to hepatic steatosis in patients with non-alcoholic fatty liver disease. Clin. Sci. 2004; 106: 635–643.
9. Bjermo H, Iggman D, Kullberg J, Dahlman I, Johansson L, Persson L, Berglund J, Pulkki K, Basu S, Uusitupa M, Rudling M, Arner P, Cederholm T, Ahlström H, Risérus U. Effects of n−6 PUFAs compared with SFAs on liver fat, lipoproteins, and inflammation in abdominal obesity: a randomized controlled trial. Am. J. Clin. Nutr. 2012; 95: 1003–1012.
10. Oosterveer MH, van Dijk TH, Tietge UJF, Boer T, Havinga R, Stellaard F, Groen AK, Kuipers F, Reijngoud D-J. High fat feeding induces hepatic fatty acid elongation in mice. PLoS One 2009; 4: e6066.
11. Levant B, Ozias M, Guilford B, Wright D. Streptozotocin-induced diabetes partially attenuates the effects of a high-fat diet on liver and brain fatty acid composition in mice. Lipids 2013; 48: 939–948.
12. Ugarte M, Brown M, Hollywood K, Cooper G, Bishop P, Dunn W. Metabolomic analysis of rat serum in streptozotocin-induced diabetes and after treatment with oral triethylenetetramine (TETA). Genome Med. 2012; 4: 35–50.
13. Ren J, Dimitrov I, Sherry AD, Malloy CR. Composition of adipose tissue and marrow fat in humans by ^{1}H NMR at 7 Tesla. J. Lipid Res. 2008; 49: 2055–2062.
14. Zancanaro C, Nano R, Marchioro C, Sbarbati A, Boicelli A, Osculati F. Magnetic resonance spectroscopy investigations of brown adipose tissue and isolated brown adipocytes. J. Lipid Res. 1994; 35: 2191–2199.
15. Hamilton G, Yokoo T, Bydder M, Cruite I, Schroeder ME, Sirlin CB, Middleton MS. *In vivo* characterization of the liver fat ^{1}H MR spectrum. NMR Biomed. 2011; 24: 784–790.
16. Hamilton G, Middleton MS, Bydder M, Yokoo T, Schwimmer JB, Kono Y, Patton HM, Lavine JE, Sirlin CB. Effect of PRESS and STEAM sequences on magnetic resonance spectroscopic liver fat quantification. J. Magn. Reson. Imaging 2009; 30: 145–152.
17. Runge J, Bakker P, Gaemers I, Verheij J, Hakvoort TM, Ottenhoff R, Nederveen A, Stoker J. Measuring liver triglyceride content in mice: non-invasive magnetic resonance methods as an alternative to histopathology. Magn. Reson. Mater. Phys. Biol. Med. 2014; 27: 317–327.
18. Peng X-G, Ju S, Qin Y, Fang F, Cui X, Liu G, Ni Y, Teng G-J. Quantification of liver fat in mice: comparing dual-echo Dixon imaging, chemical shift imaging, and ^{1}H-MR spectroscopy. J. Lipid Res. 2011; 52: 1847–1855.
19. Koelblinger C, Kršňák M, Maresch J, Wrba F, Kaczirek K, Gruenberger T, Tamandl D, Ba-Ssalamah A, Berger-Kulemann V, Weber M, Schima W. Hepatic steatosis assessment with ^{1}H-spectroscopy and chemical shift imaging at 3.0T before hepatic surgery: reliable enough for making clinical decisions? Eur. J. Radiol. 2012; 81: 2990–2995.
20. Thomsen C, Becker U, Winkler K, Christoffersen P, Jensen M, Henriksen O. Quantification of liver fat using magnetic resonance spectroscopy. Magn. Reson. Imaging 1994; 12: 487–495.
21. Hájek M, Dezortová M, Wagnerová D, Škoch A, Voska L, Hejlová I, Trunečka P. MR spectroscopy as a tool for in vivo determination of steatosis in liver transplant recipients. Magn. Reson. Mater. Phys. Biol. Med. 2011; 24: 297–304.
22. Kršňák M, Hofer H, Wrba F, Meyerspeer M, Brehm A, Lohninger A, Steindl-Munda P, Moser E, Ferenci P, Roden M. Non-invasive assessment of hepatic fat accumulation in chronic hepatitis C by 1H magnetic resonance spectroscopy. Eur. J. Radiol. 2010; 74: e60–e66.
23. Corbin IR, Furth EE, Pickup S, Siegelman ES, Delikatny EJ. *In vivo* assessment of hepatic triglycerides in murine non-alcoholic fatty liver disease using magnetic resonance spectroscopy. Biochim. Biophys. Acta 2009; 1791: 757–763.

24. Garbow JR, Lin X, Sakata N, Chen Z, Koh D, Schonfeld G. *In vivo* MRS measurement of liver lipid levels in mice. J. Lipid Res. 2004; 45: 1364–1371.
25. Ramamonjisoa N, Ratiney H, Mutel E, Guillou H, Mithieux G, Pilleul F, Rajas F, Beuf O, Cavassila S. *In vivo* hepatic lipid quantification using MRS at 7T in a mouse model of glycogen storage disease type 1a. J. Lipid Res. 2013; 54: 2010–2022.
26. Nunes PM, Wright AJ, Veltien A, van Asten JJA, Tack CJ, Jones JG, Heerschap A. Dietary lipids do not contribute to the higher hepatic triglyceride levels of fructose- compared to glucose-fed mice. FASEB J. 2014; 28: 1988–1997.
27. Ye Q, Danzer C, Fuchs A, Wolfrum C, Rudin M. Hepatic lipid composition differs between ob/ob and ob/+ control mice as determined by using *in vivo* localized proton magnetic resonance spectroscopy. Magn. Reson. Mater. Phys. Biol. Med. 2012; 25: 381–389.
28. Tkáč I, Starčuk Z, Choi IY, Gruetter R. *In vivo* ^{1}H NMR spectroscopy of rat brain at 1 ms echo time. Magn. Reson. Med. 1999; 41: 649–656.
29. Gruetter R, Tkáč I. Field mapping without reference scan using asymmetric echo-planar techniques. Magn. Reson. Med. 2000; 43: 319–323.
30. Bolan PJ, DelaBarre L, Baker EH, Merkle H, Everson LI, Yee D, Garwood M. Eliminating spurious lipid sidebands in ^{1}H MRS of breast lesions. Magn. Reson. Med. 2002; 48: 215–222.
31. Folch J, Lees M, Stanley GHS. A simple method for the isolation of total lipids from animal tissues. J. Biol. Chem. 1957; 226: 497–509.
32. Provencher SW. Automatic quantitation of localized *in vivo* ^{1}H spectra with LCModel. NMR Biomed. 2001; 14: 260–264.
33. Strobel K, van den Hoff J, Pietzsch J. Localized proton magnetic resonance spectroscopy of lipids in adipose tissue at high spatial resolution in mice in vivo. J. Lipid Res. 2008; 49: 473–480.
34. Warskulat U, Borsch E, Reinehr R, Heller-Stilb B, Mönnighoff I, Buchczyk D, Donner M, Flögel U, Kappert G, Soboll S, Beer S, Pfeffer K, Marschall H-U, Gabrielsen M, Amiry-Moghaddam M, Ottersen OP, Dienes HP, Häussinger D. Chronic liver disease is triggered by taurine transporter knockout in the mouse. FASEB J. 2006; 20: 574–576.
35. Wu C, Okar DA, Newgard CB, Lange AJ. Overexpression of 6-phosphofructo-2-kinase/fructose-2,6-bisphosphatase in mouse liver lowers blood glucose by suppressing hepatic glucose production. J. Clin. Invest. 2001; 107: 91–98.
36. Huang J, Tabbi-Anneni I, Gunda V, Wang L. Transcription factor Nrf2 regulates SHP and lipogenic gene expression in hepatic lipid metabolism. Am. J. Physiol. Gastrointest. Liver Physiol. 2010; 299: G1211–G1221.
37. Ouwerkerk R, Pettigrew RI, Gharib AM. Liver metabolite concentrations measured with ^{1}H MR spectroscopy. Radiology 2012; 265: 565–575.
38. Feng J, Isern NG, Burton SD, Hu JZ. Studies of secondary melanoma on C57BL/6J mouse liver using ^{1}H NMR metabolomics. Metabolites 2013; 3: 1011–1035.
39. Cobbold JFL, Patel JH, Goldin RD, North BV, Crossey MME, Fitzpatrick J, Wylezinska M, Thomas HC, Cox IJ, Taylor-Robinson SD. Hepatic lipid profiling in chronic hepatitis C: an *in vitro* and *in vivo* proton magnetic resonance spectroscopy study. J. Hepatol. 2010; 52: 16–24.
40. Cobbold JFL, Anstee QM, Goldin RD, Williams HRT, Matthews HC, North BV, Absalom N, Thomas HC, Thursz MR, Cox RD, Taylor-Robinson SD, Cox IJ. Phenotyping murine models of non-alcoholic fatty liver disease through metabolic profiling of intact liver tissue. Clin. Sci. 2009; 116: 403–413.
41. Martínez-Granados B, Monleón D, Martínez-Bisbal MC, Rodrigo JM, del Olmo J, Lluch P, Ferrández A, Martí-Bonmatí L, Celda B. Metabolite identification in human liver needle biopsies by high-resolution magic angle spinning ^{1}H NMR spectroscopy. NMR Biomed. 2006; 19: 90–100.
42. Alexander LR, Justice JB, Jr, Madden J. Fatty acid composition of human erythrocyte membranes by capillary gas chromatography–mass spectrometry. J. Chromatogr. B Biomed. Sci. Appl. 1985; 342: 1–12.
43. Fauland A, Köfeler H, Trötzmüller M, Knopf A, Hartler J, Eberl A, Chitraju C, Lankmayr E, Spener F. A comprehensive method for lipid profiling by liquid chromatography-ion cyclotron resonance mass spectrometry. J. Lipid Res. 2011; 52: 2314–2322.
44. Chitraju C, Trötzmüller M, Hartler J, Wolinski H, Thallinger GG, Haemmerle G, Zechner R, Zimmermann R, Köfeler HC, Spener F. The impact of genetic stress by ATGL deficiency on the lipidome of lipid droplets from murine hepatocytes. J. Lipid Res. 2013; 54: 2185–2194.
45. van Werven JR, Marsman HA, Nederveen AJ, ten Kate FJ, van Gulik TM, Stoker J. Hepatic lipid composition analysis using 3.0-T MR spectroscopy in a steatotic rat model. Magn. Reson. Imaging 2012; 30: 112–121.
46. Ye Q, Danzer CF, Fuchs A, Vats D, Wolfrum C, Rudin M. Longitudinal evaluation of hepatic lipid deposition and composition in ob/ob and ob/+ control mice. NMR Biomed. 2013; 26: 1079–1088.
47. Yaligar J, Gopalan V, Kiat OW, Sugii S, Shui G, Lam BD, Henry CJ, Wenk MR, Tai ES, Velan SS. Evaluation of dietary effects on hepatic lipids in high fat and placebo diet fed rats by *in vivo* MRS and LC-MS techniques. PLoS One 2014; 9: e91436.
48. Hu C, Hoene M, Zhao X, Häring HU, Schleicher E, Lehmann R, Han X, Xu G, Weigert C. Lipidomics analysis reveals efficient storage of hepatic triacylglycerides enriched in unsaturated fatty acids after one bout of exercise in mice. PLoS One 2010; 5: e13318.
49. Hakumäki JM, Kauppinen RA. ^{1}H NMR visible lipids in the life and death of cells. Trends Biochem. Sci. 2000; 25: 357–362.
50. Mlynárik V, Gambarota G, Frenkel H, Gruetter R. Localized short-echo-time proton MR spectroscopy with full signal-intensity acquisition. Magn. Reson. Med. 2006; 56: 965–970.
51. Yahya A, Tessier AG, Fallone BG. Effect of J-coupling on lipid composition determination with localized proton magnetic resonance spectroscopy at 9.4 T. J. Magn. Reson. Imaging 2011; 34: 1388–1396.
52. Gajdošík M, Chmelík M, Just-Kukurová I, Bogner W, Valkovič L, Trattnig S, Kršňák M. In vivo relaxation behavior of liver compounds at 7 tesla, measured by single-voxel proton MR spectroscopy. J. Magn. Reson. Imaging 2014; 40: 1365–1374.
53. Tang H, Miller C, Kennan R, Wu EX, Williams DS, Liu H. *In vivo* lipid quantitation in mouse liver using the gradient reversal water-fat imaging method. Proc. Int. Soc. Magn. Reson. Med. 2007; 15: 727.
54. Xin L, Gambarota G, Cudalbu C, Mlynárik V, Gruetter R. Single spin-echo T_2 relaxation times of cerebral metabolites at 14.1 T in the *in vivo* rat brain. Magn. Reson. Mater. Phys. Biol. Med. 2013; 26: 549–554.
55. Kim W, Rho H, Hong Y, Yeom M, Shin S, Yi J, Lee M-S, Park H, Cho D. Determination and comparison of seed oil triacylglycerol composition of various soybeans (*Glycine max* (L.)) using ^{1}H-NMR spectroscopy. Molecules 2013; 18: 14448–14454.
56. Ayorinde FO, Garvin K, Saeed K. Determination of the fatty acid composition of saponified vegetable oils using matrix-assisted laser desorption/ionization time-of-flight mass spectrometry. Rapid Commun. Mass Spectrom. 2000; 14: 608–615.
57. Duarte JAG, Carvalho F, Pearson M, Horton JD, Browning JD, Jones JG, Burgess SC. A HFD suppresses de novo lipogenesis and desaturation, but not elongation and triglyceride synthesis in mice. J. Lipid Res. 2014; 55: 2541–2553.
58. Nishida M, Sasaki T, Terada H, Kawada J. A signoidal relationship between liver stearoyl CoA desaturase activity and serum hormone concentrations caused by streptozocin and its antagonists. Experientia 1988; 44: 756–758.
59. Wang Y, Botolin D, Xu J, Christian B, Mitchell E, Jayaprakasam B, Nair M, Peters JM, Busik J, Olson LK, Jump DB. Regulation of hepatic fatty acid elongase and desaturase expression in diabetes and obesity. J. Lipid Res. 2006; 47: 2028–2041.
60. van Hoeven RP, Emmelot P. Studies on plasma membranes: XVIII. Lipid class composition of plasma membranes isolated from rat and mouse liver and hepatomas. J. Membr. Biol. 1972 9: 105–126.
61. Abbott SK, Else PL, Atkins TA, Hulbert AJ. Fatty acid composition of membrane bilayers: importance of diet polyunsaturated fat balance. Biochim. Biophys. Acta 2012; 1818: 1309–1317.
62. Bohov P, Šeböková E, Gašperíková D, Langer P, Klimeš I. Fatty acid composition in fractions of structural and storage lipids in liver and skeletal muscle of hereditary hypertriglyceridemic rats. Ann. N. Y. Acad. Sci. 1997; 827: 494–509.
63. Vázquez M, Alegret M, López M, Rodriguez C, Adzet T, Merlos M, Laguna JC. Different effects of fibrates on the microsomal fatty acid chain elongation and the acyl composition of phospholipids in guineapigs. Br. J. Pharmacol. 1995; 116: 3337–3343.
64. Giarola M, Rossi B, Mosconi E, Fontanella M, Marzola P, Scambi I, Sbarbati A, Mariotto G. Fast and minimally invasive determination of the unsaturation index of white fat depots by micro-Raman spectroscopy. Lipids 2011; 46: 659–667.
65. Mitchell TW, Buffenstein R, Hulbert AJ. Membrane phospholipid composition may contribute to exceptional longevity of the naked mole-rat (*Heterocephalus glaber*): a comparative study using shotgun lipidomics. Exp. Gerontol. 2007; 42: 1053–1062.

66. Koc H, Mar M-H, Ranasinghe A, Swenberg JA, Zeisel SH. Quantitation of choline and its metabolites in tissues and foods by liquid chromatography/electrospray ionization-isotope dilution mass spectrometry. Anal. Chem. 2002; 74: 4734–4740.
67. Abrigo JM, Shen J, Wong VWS, Yeung DKW, Wong GLH, Chim AML, Chan AWH, Choi PCL, Chan FKL, Chan HLY, Chu WCW. Non-alcoholic fatty liver disease: spectral patterns observed from an *in vivo* phosphorus magnetic resonance spectroscopy study. J. Hepatol. 2014; 60: 809–815.
68. Meftah NM, Skett P. The role of microsomal phospholipids and their fatty acid composition in the control of hepatic metabolism of lignocaine. Br. J. Pharmacol. 1989; 98: 1399–1405.
69. Shin CS, Lee MK, Park KS, Kim SY, Cho BY, Lee HK, Koh CS, Min HK. Insulin restores fatty acid composition earlier in liver microsomes than erythrocyte membranes in streptozotocin-induced diabetic rats. Diabetes Res. Clin. Pract. 1995; 29: 93–98.